

www.acsaem.org Article

# Solvent-Cast Solid Electrolyte Membranes Based on a Charged Rigid-Rod Polymer and Ionic Liquids

Deyang Yu, Curt J. Zanelotti, Ryan J. Fox, Theo J. Dingemans, and Louis A. Madsen\*



Cite This: ACS Appl. Energy Mater. 2021, 4, 6599–6605



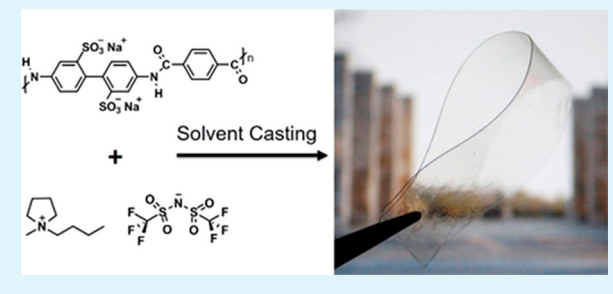
**ACCESS** 

III Metrics & More

Article Recommendations

s Supporting Information

**ABSTRACT:** Solid-state electrolytes are attractive for use in electrochemical devices because they remove the need for a flammable liquid electrolyte while contributing to the structural integrity of the device. We have recently developed a class of solid electrolytes, termed molecular ionic composites (MICs), composed of ionic liquids (ILs) and a rigid-rod polyelectrolyte, poly(2,2'-disulfonyl-4,4'-benzidine terephthalamide) (PBDT). MIC materials, originally obtained through an ion-exchange process between IL and PBDT aqueous solution, possess an unprecedented combination of high ionic conductivity, high thermal stability, low flammability, and widely tunable tensile storage



moduli. Here we present a facile solvent casting method for preparing MIC membranes. These membranes are uniform, flexible, and tough, with tunable composition and thickness ( $\geq$ 40  $\mu$ m). Unlike the previous ion-exchange method, which only allowed incorporation of hydrophilic ILs, we can now incorporate hydrophobic ILs to prepare MIC membranes for, for example, battery electrolytes. A sodium (Na) metal symmetric cell constructed with a PBDT-Pyr<sub>14</sub> TFSI membrane as the solid electrolyte shows long-term stable cycling (>500 h) at 60 °C. The ability to prepare MICs by using both hydrophilic and hydrophobic ILs initiates a wider range of MIC materials and broadens the array of applications accessible by MIC membranes.

**KEYWORDS:** ion gel, high temperature, polymer electrolyte, liquid crystalline polymer, solid-state battery

## 1. INTRODUCTION

Ionic liquid gel polymer electrolytes (ILGPEs), made by immobilizing an ionic liquid (IL) in a polymer matrix, have received increasing attention due to their potential applications in electrochemical devices.<sup>1-9</sup> A large variety of flexible (co)polymers, such as PVDF-HFP,<sup>7,10,11</sup> PMMA,<sup>1,12</sup> PS-r-PMMA, 13 and PS-b-PEO-b-PS, 14 have been explored to construct ILGPEs. However, because of the trade-off between mechanical properties and ionic conductivity, the preparation of ILGPEs with both high ionic conductivity and robust mechanical properties remains challenging. 13,15,16 And in many cases, the ILGPE melts at elevated temperature due to the increased solubility of the polymer matrix in the corresponding IL. 2,8,10 ILGPEs made from rigid polymers, such as methyl cellulose and sulfonated polyimide, demonstrate high tensile moduli at low polymer content and thus might be a potential solution to this trade-off.<sup>3,17-20</sup> Recently, our group has developed a new class of solid electrolyte, termed molecular ionic composites (MICs), composed of ILs and poly(2,2'disulfonyl-4,4'-benzidine terephthalamide) (PBDT). 21-23 PBDT is a sulfonated aromatic polyamide that shows a rigid double-helical conformation in aqueous solution and in MIC electrolytes, as shown in Figure 1a. 21,24 In MICs, the mobile cations and anions of the IL form alternating layers around the negatively charged rigid PBDT rods.<sup>25</sup> MICs show an unprecedented combination of properties: widely tunable

tensile storage modulus (0.03–3 GPa), high ionic conductivity ( $\sim$ 1 mS/cm), and high thermal stability (up to 300 °C), <sup>21,22</sup> making this MIC material a new solid electrolyte design platform.

Previously, we have fabricated millimeter-scale "ingots" of MIC materials via an ion-exchange process between an IL and a PBDT aqueous solution in small diameter glass tubes. However, many applications will require electrolytes in the form of uniform planar membranes. The previous ion-exchange process involves the interfacial combination of two phases, a polymer solution and neat IL, and so making a uniform thin membrane is difficult. Another major limitation of the ion-exchange process is that both the IL and PBDT must be miscible with the solvent used to prepare the PBDT solution. Therefore, when using water as the solvent, the IL incorporated must be hydrophilic, and this severely limits the use of ILs that are known to perform well in lithium/sodium batteries, such as the hydrophobic 1-methyl-1-propyl-

Received: March 4, 2021 Accepted: June 14, 2021 Published: June 30, 2021





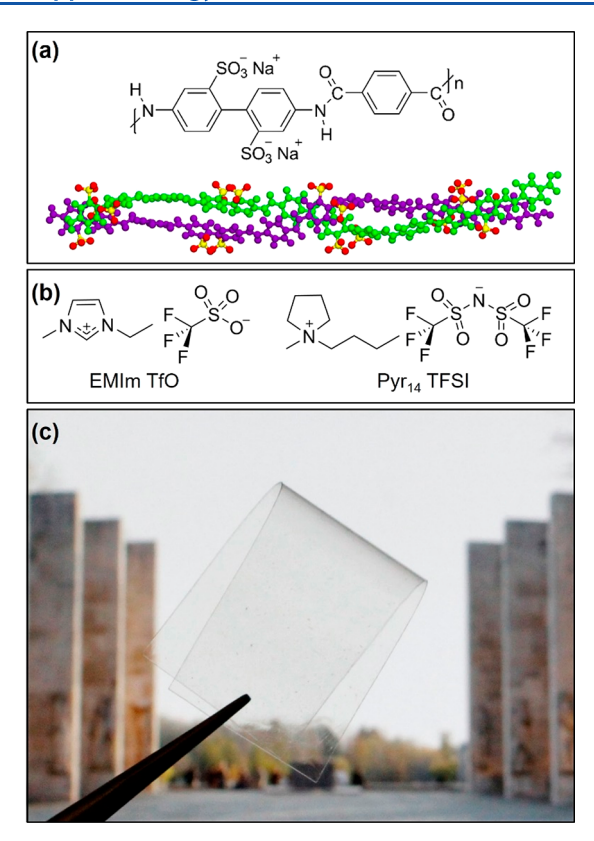


**Figure 1.** (a) Chemical structure of PBDT and the PBDT double helix. (b) Chemical structures of EMIm TfO and Pyr<sub>14</sub> TFSI ILs. (c) Image of a MIC membrane containing 20 wt % PBDT and 80 wt % Pyr<sub>14</sub> TFSI with thickness =  $90 \pm 5 \mu m$ . MIC membranes prepared from PBDT and ILs are transparent, flexible, and tough.

piperidinium TFSI and 1-alkyl-1-methylpyrrolidinium TFSI.<sup>26,27</sup>

Solvent casting is a common method for preparing ILGPEs. Typically the polymer and IL are dissolved in a common solvent to make a casting solution. Spreading the casting solution on a substrate followed by solvent evaporation results in a uniform ILGPE membrane. Although many flexible polymers have been used to prepare ILGPEs, rigid polymers have not been widely studied primarily because of their limited solubility in common solvents, originating from their lower entropy increase during dissolution compared to flexible polymers. Solvent mixtures are scarcely used in the preparation of ILGPEs, and yet employing solvent mixtures in

casting processes can often influence the final membrane morphology. In this article, we demonstrate the self-assembly of rigid PBDT and ILs in both single solvent and solvent mixtures to yield uniform and flexible membranes through solvent casting. We also investigate the morphology of the obtained MIC membranes. Finally, a sodium (Na) symmetric cell constructed with a MIC electrolyte shows stable long-term cycling performance relevant to sodium—metal batteries.

## 2. EXPERIMENTAL SECTION

Materials. PBDT was synthesized as previously reported. 32,33 PBDT aqueous solution shows a transition from isotropic to mixed isotropic/nematic at 1.1 wt % and then to fully nematic phase at ≥1.8 wt % PBDT. 1-Ethyl-3-methylimidazolium trifluoromethanesulfonate (EMIm TfO, 99%) and 1-butyl-1-methylpyrrolidinium bis(trifluoromethylsulfonyl)imide (Pyr₁4 TFSI, 99%) were purchased from Iolitec Inc. (Germany) and used as received. *N,N*-Dimethylformamide (DMF) was purchased from Fisher Scientific and used as received.

Membrane Preparation. The following procedures were conducted to prepare a MIC membrane that contains 10 wt % PBDT and 90 wt % EMIm TfO. 0.05 g of PBDT was dissolved in 6.0 g of H<sub>2</sub>O in a glass vial. 0.45 g of EMIm TfO was dissolved in another 6.0 g of H<sub>2</sub>O in a separate glass vial. Both solutions were heated to 85 °C and then mixed together. The mixed solution, which contains 0.05 g of PBDT, 0.45 g of EMIm TfO, and 12.0 g of H<sub>2</sub>O, was termed as the casting solution. After equilibrating at 85 °C overnight in a tightly capped glass vial inside a Yamato DX600 oven, the casting solution was poured onto a flat glass substrate preheated to 85 °C and dried at 85 °C in the oven at atmospheric pressure for 24 h. A self-standing dry MIC membrane, which is termed 10 wt % PBDT-EMIm TfO, was obtained after further drying of the membrane in a vacuum oven at 100 °C for 2 days. The membrane thickness could be controlled through the amount of material used and the size of the casting substrate and can range from 40 to 600 µm. MIC membranes made from Pyr<sub>14</sub> TFSI were prepared in a similar way except that equal masses of H<sub>2</sub>O and DMF were used as solvent for PBDT and ionic liquid, respectively. Table 1 shows the mass of each chemical used to prepare each MIC membrane. The complete removal of DMF (to an upper limit of 0.1 wt %) in PBDT-Pyr<sub>14</sub> TFSI membranes after vacuum drying was examined by <sup>1</sup>H NMR (Figure S1).

**Characterizations.** Differential scanning calorimetry (DSC) was measured with a TA Instruments DSC Q100 with liquid nitrogen gas cooling accessory. PBDT-EMIm TfO samples were heated to 200 °C and equilibrated at 200 °C for 5 min to fully eliminate water. During cooling to −130 °C, the temperature was held at −15, −30, and −45 °C for 10 min to allow the ionic liquid to fully crystallize (the following heating curve shows no crystallization peak, Figure S5). The second heating curve from −130 to 50 °C at 10 °C/min is reported in Figure S5. For PBDT-Pyr₁4 TFSI samples, after the first heating to 200 °C and cooling to −130 °C, they were heated to −25 °C and

Table 1. Summary of Casting Solution Compositions upon Initial Mixing and at the Gel Point

ionic liquid	mass of IL (g)	mass of PBDT (g)	$\begin{array}{c} \text{mass of } H_2O \\ \text{(g)} \end{array}$	mass of DMF (g)	polymer (solute <sup>a</sup> ) content at gel point <sup>b</sup>	mass ratio of DMF to $H_2O$ at gel point $^c$	MIC membrane <sup>d</sup>
EMIm TfO	0.45	0.050	12.0	N/A	2.1 wt % (21%)	N/A	10 wt % EMIm TfO
EMIm TfO	0.40	0.10	12.0	N/A	4.2 wt % (21%)	N/A	20 wt % EMIm TfO
Pyr <sub>14</sub> TFSI	0.45	0.050	5.0	5.0	0.78 wt % (7.8%)	2.8:1	10 wt % Pyr <sub>14</sub> TFSI
Pyr <sub>14</sub> TFSI	0.40	0.10	5.0	5.0	1.5 wt % (7.5%)	2.3:1	20 wt % Pyr <sub>14</sub> TFSI
Pyr <sub>14</sub> TFSI	0.35	0.15	5.0	5.0	2.2 wt % (7.3%)	2.3:1	30 wt % Pyr <sub>14</sub> TFSI

<sup>&</sup>quot;Solute includes both PBDT and IL. <sup>b</sup>Gel point defined as the composition at which the solution has lost its ability to flow at 85 °C. <sup>c</sup>Gel point composition determined from <sup>1</sup>H NMR integration by dissolving the gel in D<sub>2</sub>O. <sup>d</sup>Weight percent denotes the content of PBDT in the fully dried final membrane.

equilibrated at  $-25~^\circ C$  for 20 min to allow full crystallization of ionic liquid. The 10 wt % PBDT-Pyr $_{14}$  TFSI samples were equilibrated for another 20 min at  $-35~^\circ C$  to allow full crystallization of the IL. After cooling to  $-130~^\circ C$ , the third heating trace at  $10~^\circ C/\text{min}$  was reported. Electrochemical impedance spectroscopy (EIS) was performed on a BioLogic SP-200 instrument with an AC bias of 10 mV. Samples were first cut into disks and sandwiched between two stainless steel plates and then assembled into standard 2032-type coin cells in an Ar-filled glovebox. The ionic conductivity was calculated via the equation

$$\sigma = \frac{l}{R \times A} \tag{1}$$

where  $\sigma$  (expressed in S/cm) is the ionic conductivity, l (expressed in cm) is the thickness of the membrane, A (expressed in cm²) is the contact area between stainless steel and the membrane, and R (expressed in  $\Omega$ ) is the bulk resistance of the membrane. Thermogravimetric analysis (TGA) was measured with a TA Instruments TGA Q500 in a dry  $N_2$  atmosphere and with a heating rate of 10 °C/min. Stress—strain tests were measured on a TA Instruments DMA Q800 at room temperature with a strain rate of 1%/min. Dynamic mechanical thermal analysis was measured in the same way as previously reported. Polarized optical microscopy (POM) was measured on a Meiji techno MX microscope with an Infinity digital camera. We conducted sodium symmetric cell cycling on a Neware battery test system using a galvanostatic cycling protocol.

## 3. RESULTS AND DISCUSSION

As mentioned earlier, rigid polymers usually have limited solubility. However, PBDT is a water-miscible polymer because it has two sulfonate groups per repeat unit, as shown in Figure 1a. PBDT aqueous solution forms a nematic liquid crystalline (LC) phase when its concentration is above  $\sim$ 1 wt %, depending on the polymer molecular weight. <sup>22,23,34</sup> 1-Ethyl-3-methylimidazolium trifluoromethanesulfonate (EMIm TfO) is a water-miscible IL (Figure 1b). When EMIM TfO is mixed directly with PBDT aqueous solution, a heterogeneous gel forms quickly. The method used to prevent formation of this heterogeneous gel and obtain a liquid casting solution is to dissolve both PBDT and EMIm TfO separately in equal masses of water (Table 1) at elevated temperature (>80 °C) followed by mixing. Once mixed, we hold the casting solution at this elevated temperature to ensure complete dissolution. We then obtain free-standing membranes by drying the casting solution on a flat glass substrate (Figure 2a). We can also prepare MIC membranes from hydrophobic ILs, as exemplified by incorporating 1-butyl-1-methylpyrrolidinium bis(trifluoromethylsulfonyl)imide (Pyr<sub>14</sub> TFSI, Figure 1b). Water-miscible N,N-dimethylformamide (DMF) dissolves  $Pyr_{14}$  TFSI to form the IL part of the casting solution. We then cast the PBDT-Pyr<sub>14</sub> TFSI membrane from a cosolvent of H<sub>2</sub>O and DMF after mixing the PBDT aqueous solution and IL-DMF solution at 85 °C. Figure 1c shows a strip of the PBDT-Pyr<sub>14</sub> TFSI membrane. The amount of residual DMF in the membrane is minimal after drying the membrane at 100 °C under vacuum for 2 days, as confirmed by <sup>1</sup>H NMR (Figure

Although elevated temperature helps prevent the liquid casting solution from gelling, the casting solution still forms a gel during the solvent evaporation process. The weight percent of solute (PBDT and IL) at the gel point at 85 °C is 21 and <8 wt % for the EMIm TfO and Pyr<sub>14</sub> TFSI systems, respectively (Table 1). Thus, the combination of elevated temperature and initially low solute content is the key to successfully preparing liquid casting solutions and then obtaining MIC membranes.

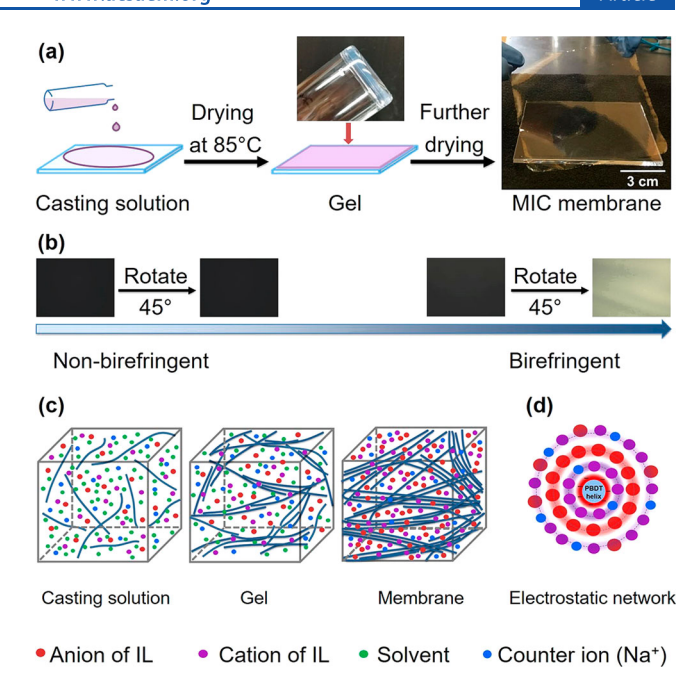


Figure 2. Schematic illustration of the solvent casting process and formation of PBDT-IL associated "bundle" phase and IL-rich "puddle" phase during solvent evaporation. (a) Solvent casting process for forming MIC membranes. Casting consists of mixing a PBDT aqueous solution and an IL solution at 85 °C followed by pouring onto a glass substrate preheated to 85 °C. The solution solidifies during solvent evaporation as the solution passes the gel point. To obtain uniform and robust films, the solution must exceed the PBDT concentration for forming the nematic liquid crystalline (LC) phase. After complete drying, a self-standing membrane easily peels off the glass substrate. (b) POM images of the casting solution and dry MIC membrane. The casting solution is nonbirefringent while the dry membrane is birefringent, indicating alignment of PBDT rods as solvent evaporation occurs. (c) Conceptual illustrations of the casting process at different stages. In the casting solution, PBDT double helices (blue lines) and IL are dispersed homogeneously. During drying, PBDT double helices coagulate and locally align with the aid of electrostatic interactions, causing polymer chain percolation through the whole solution and leading to formation of a LC gel. Upon further drying, coagulated rods form the PBDT-IL associated "bundle" phase while free IL not incorporated into the bundle phase forms the IL-rich "puddle" phase. (d) Scheme of the alternating ionic layers around a PBDT double helix. When viewed down the PBDT rigid-rod axis, cations and anions form alternating layers around the negatively charged PBDT axis.

We fixed the solvent evaporation process at 85 °C instead of a higher temperature to prevent more rapid solvent evaporation which can lead to trapped bubbles.

MIC membranes prepared in this way are flexible and handleable, allowing for excessive twisting and bending, and are uniform without any noticeable pinholes. On the basis of the simplicity of this casting method, we can easily tune the thickness of the membrane (40–600  $\mu$ m) and the membrane area by adjusting the total amount of solution and the film casting area. Figure 2a shows a MIC membrane of 10 × 10 cm<sup>2</sup>.

Previous morphology studies on PBDT-EMIm TfO MICs reveal that the MIC membranes demonstrate a biphasic structure composed of a PBDT-IL associated bundle phase (polymer-rich phase) and an IL-rich puddle phase (IL-rich phase).<sup>22,23</sup> Here we propose a model regarding the formation

of this biphasic structure with respect to the current solvent casting process.

In the initial (relatively dilute) casting solution, doublehelical PBDT rods disperse homogeneously with no preferred polymer orientational order, as evidenced by the lack of birefringence of the casting solution when examined by polarized optical microscopy (POM) (Figure 2b). As solvent evaporates, the concentration of PBDT in the solution increases and the rods start to locally align when the concentration of PBDT exceeds a critical value. The interaction between polymer and IL contributes to the coagulation of PBDT chains, leading to the formation of PBDT-IL bundles. The bundles are liquid crystalline due to the high rigidity of the PBDT rigid rods, presumably similar in character to the formation of aligned aggregates of polybenzimidazole during polyphosphoric acid hydrolysis. 35,36 IL molecules not incorporated into polymer bundles are freely dissolved in the solvent to form a separate liquid phase. As solvent evaporation continues, a percolating network of PBDT-IL bundles leads to formation of a LC gel. Upon further evaporation, bundles pack more closely to form a continuous mechanically robust network of polymer and IL, which is the PBDT-IL associated bundle phase in the MIC membrane. The PBDT-IL bundles exhibit liquid crystalline order as evidenced by the bright-dark alternation over a large area every 45° under POM (Figure S2). Our previous work showed that the PBDT-IL bundles have a strong in-plane orientation caused by the reduction of the thickness of the gel network during solvent evaporation. 22 IL not incorporated into the PBDT-IL bundle phase, which presumably has a thermodynamically optimized packing fraction, forms the IL-rich puddle phase.<sup>23</sup> The mass ratio of PBDT to IL affects the relative amount of PBDT-IL bundle phase and IL puddle phase. Differential scanning calorimetry (DSC) measurements (ref 22 and Figure S5) show that the IL crystallinity in PBDT-EMIm TfO membranes decreases as polymer content increases, and the melting peak of IL disappears when the polymer content is above 20 wt %. This behavior reinforces the idea that the ILrich "puddle" phase tends to reduce and disappear as PBDT content increases.

Turning to a hydrophobic IL with potential applications in battery electrolytes, Pyr<sub>14</sub>TFSI shows a complicated phase behavior due to the formation of a polymorphic crystalline phase.<sup>37–40</sup> Previous researchers reported that the DSC heating trace of Pyr<sub>14</sub>TFSI after quenching shows multiple transitions, including a glass transition at -87 °C, a recrystallization peak around -50 °C, a solid-solid phase transition at about -24 °C, and a melting peak at -18 °C.<sup>40</sup> The heating trace of Pyr<sub>14</sub>TFSI after slow cooling only shows a melting transition at -7 °C, <sup>39</sup> although the melting peak could shift to -3 °C when the IL is fully crystalline.<sup>38</sup> To allow crystallization of IL in PBDT-Pyr<sub>14</sub> TFSI membranes and thus simplify the heating traces, we annealed these samples at -25°C for 20 min. The 10 wt % PBDT-Pyr<sub>14</sub> TFSI sample required another 20 min of annealing at  $-35\,^{\circ}\text{C}$  due to the broadness of its melting peak at −20 °C. Figure 3 shows DSC heating traces of PBDT-Pyr<sub>14</sub> TFSI membranes after crystallization. The small distortion of these curves (spikes) around -29 °C is an artifact as it is observed in all of the samples including PBDT-EMIm TfO membranes (Figure S5). The glass transition temperature of the IL in these membranes is -84 °C. The 10 wt % PBDT-Pyr<sub>14</sub> TFSI sample shows two melting peaks (-20 and -9 °C), while for higher polymer

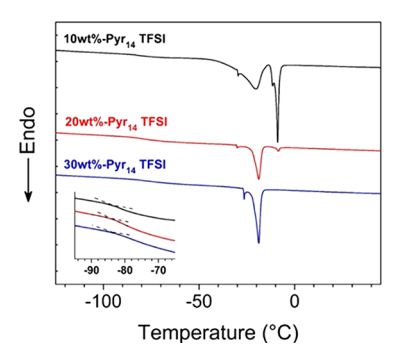


Figure 3. DSC heating traces (10 °C/min) of PBDT-Pyr $_{14}$  TFSI membranes after annealing at -25 °C for 20 min. The inset shows the enlarged glass transition region and determination of  $T_{\rm g}$ . We vertically normalized these traces using the mass of IL in each sample. We attribute the glass transition temperature observed at -84 °C (inset) to the IL in the PBDT-IL associated bundle phase. We assign the melting peaks to the IL in the IL-rich puddle phase. Note that we applied an additional 20 min annealing at -35 °C to the 10 wt % PBDT-Pyr $_{14}$  TFSI sample to eliminate the crystallization peak in the following heating process.

content samples we see only a single melting peak at -19 °C. As opposed to the PBDT-EMIm TfO MICs, the IL melting peak position in these PBDT-Pyr<sub>14</sub> TFSI membranes is almost identical with the melting point of neat IL suggesting a weaker interaction between the IL and PBDT and/or weaker confinement.

Another difference between PBDT-Pyr<sub>14</sub> TFSI membranes as compared to PBDT-EMIm TfO is that the IL melting peak is present even when the polymer content is as high as 30 wt %. We believe this relates to the slow evaporation rate of DMF compared to water. During the solvent evaporation process, DMF becomes more and more concentrated, contributing to the phase separation between PBDT-IL bundles and the liquid phase. Indeed, DMF is a poor solvent for PBDT. The enrichment of DMF relative to water during drying makes the liquid phase a better solvent for the hydrophobic Pyr<sub>14</sub> TFSI, leading to a more pronounced IL puddle phase in the MIC membrane. Thus, the biphasic structure of PBDT-Pyr<sub>14</sub> TFSI membranes depends not only on the relative amount of polymer and IL but also on the nature of the solvent.

Mechanical strength is critical for an ILGPE when considering large-scale manufacturing criteria. 41,42 The Young's moduli of PBDT-Pyr<sub>14</sub> TFSI membranes containing 10, 20, and 30 wt % polymer are 0.53, 1.7, and 2.6 GPa, respectively (Figure 4a). These high tensile moduli are comparable to PBDT-EMIm TfO membranes.<sup>22</sup> Uniaxial stress-strain measurements show the existence of a plastic deformation region above ~1% strain for PBDT-Pyr<sub>14</sub> TFSI membranes. This plastic deformation may be due to the plasticizing effect of this hydrophobic IL and potentially residual casting solvents at ~1 wt % or lower content. The reorientation of the polymer bundles in PBDT-Pyr<sub>14</sub> TFSI, where the biphasic structure is more pronounced, with applied strain may be another possible explanation for this plastic deformation. Because of the presence of this plastic deformation, the tensile strength of 20 wt % PBDT-Pyr<sub>14</sub> TFSI is larger than the 20 wt % PBDT-EMIm TfO membrane by a factor of 2.8.

Dynamic mechanical thermal analysis (DMTA) provides further evaluation of the mechanical stability of MIC membranes at elevated temperatures. Figure 4b shows tensile

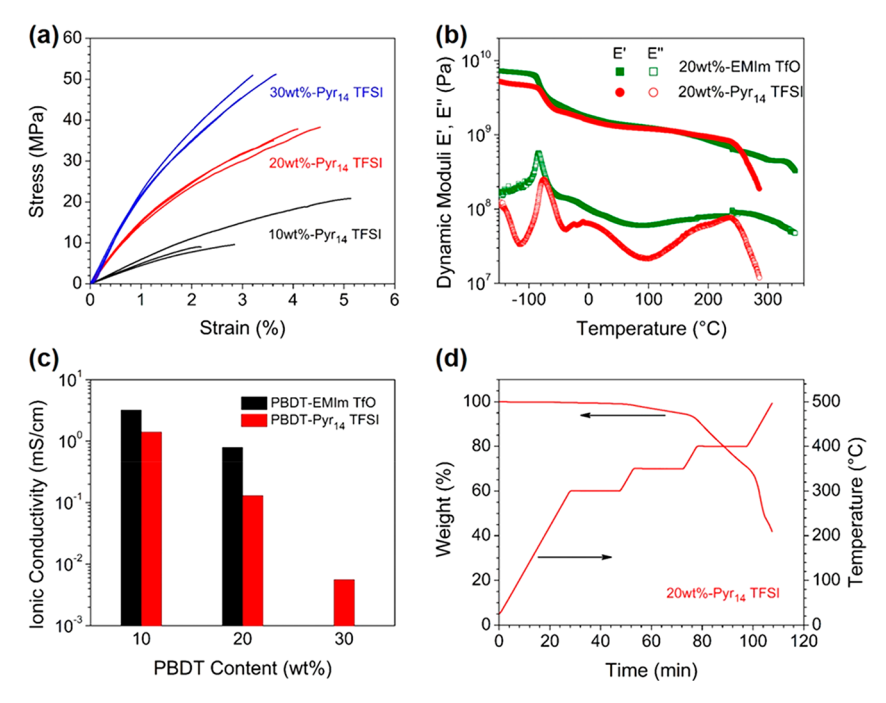


Figure 4. Mechanical properties, ionic conductivity, and thermal stability of MIC membranes. (a) Uniaxial stress—strain test of PBDT-Pyr $_{14}$  TFSI membranes at a strain rate of 1% min $^{-1}$  at room temperature, with measurement of each sample repeated three times. The slope of the stress—strain curves at <0.5% yields the Young's modulus. (b) Dynamic moduli (E' and E'') of 20 wt % PBDT-EMIm TfO and 20 wt % PBDT-Pyr $_{14}$  TFSI membranes measured at a heating rate of 2 °C/min at an oscillation frequency of 1 Hz and 0.1% strain. (c) Ionic conductivity of MIC membranes at room temperature as a function of PBDT content. The 30 wt % PBDT-EMIm TfO sample exhibits heterogeneity and is not measured. (d) Thermogravimetric analysis (TGA) curves of 20 wt % PBDT-Pyr $_{14}$  TFSI membrane under a heating ramp with three temperature steps.

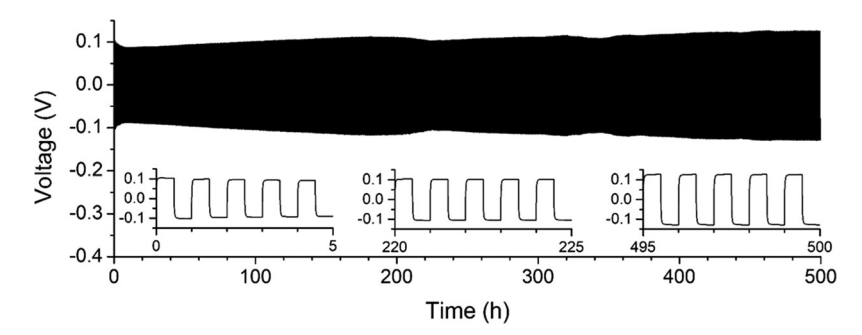


Figure 5. Voltage profile of Na/Na symmetric cell cycled at 60 °C at a current density of 0.3 mA/cm<sup>2</sup> with a solid MIC electrolyte membrane (11 wt % PBDT-Pyr<sub>14</sub> TFSI) having a thickness of 75  $\mu$ m. The charge and discharge times for each cycle are 0.5 h each. The insets show enlarged profiles for selected cycles.

storage and loss moduli for 20 wt % PBDT-EMIm TfO and 20 wt % PBDT-Pyr<sub>14</sub> TFSI over a wide temperature range. The decrease of storage modulus at about  $-80~^{\circ}$ C arises from the IL  $T_{\rm g}$ . Room temperature storage moduli for these two membranes are 1.4–1.5 GPa, and their storage moduli are >0.8 GPa even at 200 °C, demonstrating that the high rigidity of MIC membranes is preserved at high temperatures. The drop in E' and E'' for 20 wt % PBDT-Pyr<sub>14</sub> TFSI above 240 °C is likely caused by the plasticizing effect of the IL due to the changing interactions between PBDT and Pyr<sub>14</sub> TFSI at such high temperatures. Although the IL differs in these two samples, their storage moduli are very close to each other at temperatures above the IL glass transition and below 240 °C, suggesting that the stiffness mainly originates from the PBDT-IL associated bundle phase.

In addition to ease of fabrication and robust mechanical properties, electrochemical applications such as batteries also require fast ion transport. Figure 4c shows the ionic

conductivity of these MIC membranes at room temperature. When the polymer content is 10 wt %, the ionic conductivity is over 1 mS/cm. Conductivity decreases significantly with increasing polymer content. However, since membranes containing 10 and 20 wt % PBDT show high tensile strength and high Young's moduli, it may not be necessary to use a membrane with higher polymer content. We include comparisons of these ionic conductivity results with our previously published results on bulk-fabricated MICs in the Supporting Information. PBDT-Pyr<sub>14</sub> TFSI membranes exhibit slower ion transport than PBDT-EMIm TfO primarily because of the higher viscosity of Pyr<sub>14</sub> TFSI.

Furthermore, the thermal stability of solid electrolytes can also greatly contribute to the safety of electrochemical devices. <sup>43</sup> PBDT polymer shows extreme thermal stability, with a 5% mass loss temperature as high as 500 °C. <sup>22</sup> Because these ILs also show high thermal stability, the 5% mass loss temperatures of PBDT-Pyr<sub>14</sub> TFSI membranes are 380 °C

(Figure S7), similar to the PBDT-EMIm TfO membranes.<sup>22</sup> Figure 4d shows negligible mass loss for 20 wt % PBDT-Pyr<sub>14</sub> TFSI membrane after holding temperature at 300 °C for 20 min, further demonstrating the high thermal stability of MIC membranes.

To further investigate the viability of these MIC membranes as solid electrolytes, we constructed sodium (Na) metal symmetric cells using an 11 wt % PBDT-Pyr<sub>14</sub> TFSI membrane as the solid electrolyte. We cycled these cells using a current density of 0.3 mA/cm² at 60 °C. Figure 5 shows the voltage profile over 500 h cycling. The voltage trace shows no evidence of short circuit, and the polarization voltage only shows slight increase over time, demonstrating that the interface between Na and the MIC membrane has long-term stability at 60 °C. The successful cycling of Na symmetric cells also demonstrates that the mechanical properties of MIC membranes with low polymer content are sufficient to support their application as solid electrolytes in next-generation batteries.

## 4. CONCLUSIONS

In summary, we have successfully prepared uniform MIC membranes by developing a straightforward solvent casting method. By adjusting the casting solvent(s) used, we can prepare MIC membranes that incorporate both hydrophilic and hydrophobic ILs, greatly expanding the choices of ILs and enabling a broader range of applications. It is noteworthy that we can use other ILs such as N-propyl-N-methylpyrrolidinium bis(fluorosulfonyl)imide (Pyr<sub>13</sub> FSI) and 1-butyl-3-methylimidazolium bis(trifluoromethylsulfonyl)imide (BMIm TFSI) to prepare MIC membranes in the same way. A third component such as a lithium salt or sodium salt can also be incorporated into MIC membranes through this robust and versatile casting method. These membranes are highly flexible and robust, with widely tunable composition and thickness. Preliminary Na symmetric cell tests illustrate that MIC membranes prepared through this casting method can yield long-term stable cycling performance. Furthermore, detailed evaluation of MIC membranes as solid electrolytes for lithium metal batteries has recently been published elsewhere.<sup>44</sup> This simple solvent casting method makes it possible to explore the applications of MIC materials in the form of uniform thin membranes in many other fields, such as fuel cells, gas separations, and electrochemical sensors and transducers. The fact that solvent mixtures can produce more pronounced phase separation in MIC membranes than those cast from a single solvent also holds great promise for fine control over the solid electrolyte membrane morphology.

## ASSOCIATED CONTENT

## Supporting Information

The Supporting Information is available free of charge at https://pubs.acs.org/doi/10.1021/acsaem.0c03133.

Comparison of ionic conductivity between MIC membrane and MIC ingots, additional POM images, DSC and TGA traces (PDF)

# **■** AUTHOR INFORMATION

## **Corresponding Author**

Louis A. Madsen — Macromolecules Innovation Institute and Department of Chemistry, Virginia Tech, Blacksburg, Virginia 24061, United States; orcid.org/0000-0003-4588-5183; Email: lmadsen@vt.edu

### **Authors**

Deyang Yu — Macromolecules Innovation Institute and Department of Chemistry, Virginia Tech, Blacksburg, Virginia 24061, United States; ⊚ orcid.org/0000-0003-0587-1211

Curt J. Zanelotti — Macromolecules Innovation Institute and Department of Chemistry, Virginia Tech, Blacksburg, Virginia 24061, United States; ⊙ orcid.org/0000-0003-2622-7345

Ryan J. Fox — Department of Applied Physical Sciences, University of North Carolina at Chapel Hill, Chapel Hill, North Carolina 27599-3050, United States; ocid.org/ 0000-0002-1472-6262

Theo J. Dingemans — Department of Applied Physical Sciences, University of North Carolina at Chapel Hill, Chapel Hill, North Carolina 27599-3050, United States;
ocid.org/0000-0002-8559-2783

Complete contact information is available at: https://pubs.acs.org/10.1021/acsaem.0c03133

#### Notes

The authors declare no competing financial interest.

# ACKNOWLEDGMENTS

This work was supported by the National Science Foundation under Award DMR 1810194. Any opinions, findings, and conclusions or recommendations expressed in this material are those of the author(s) and do not necessarily reflect the views of the NSF. This work was also supported by the U.S. Department of Energy's Office of Energy Efficiency and Renewable Energy under Award DE-EE0008860. We gratefully acknowledge Prof. Feng Lin for his support in coin cell preparation and cycling tests. We gratefully acknowledge Dr. Yadong He for providing the PBDT double-helix figure.

# **■ REFERENCES**

- (1) Susan, M. A. B. H.; Kaneko, T.; Noda, A.; Watanabe, M. Ion Gels Prepared by in Situ Radical Polymerization of Vinyl Monomers in an Ionic Liquid and Their Characterization as Polymer Electrolytes. *J. Am. Chem. Soc.* **2005**, *127* (13), 4976–4983.
- (2) Lodge, T. P. Materials science A unique platform for materials design. *Science* **2008**, *321* (5885), 50–51.
- (3) Mantravadi, R.; Chinnam, P. R.; Dikin, D. A.; Wunder, S. L. High Conductivity, High Strength Solid Electrolytes Formed by in Situ Encapsulation of Ionic Liquids in Nanofibrillar Methyl Cellulose Networks. *ACS Appl. Mater. Interfaces* **2016**, 8 (21), 13426–13436.
- (4) Guo, P.; Su, A.; Wei, Y.; Liu, X.; Li, Y.; Guo, F.; Li, J.; Hu, Z.; Sun, J. Healable, Highly Conductive, Flexible, and Nonflammable Supramolecular Ionogel Electrolytes for Lithium-Ion Batteries. *ACS Appl. Mater. Interfaces* **2019**, *11* (21), 19413–19420.
- (5) Sun, N.; Gao, X.; Wu, A.; Lu, F.; Zheng, L. Mechanically strong ionogels formed by immobilizing ionic liquid in polyzwitterion networks. *J. Mol. Liq.* **2017**, *248*, 759–766.
- (6) Zhao, X.; Guo, S.; Li, H.; Liu, J.; Liu, X.; Song, H. In Situ Synthesis of Imidazolium-Crosslinked Ionogels via Debus—Radziszewski Reaction Based on PAMAM Dendrimers in Imidazolium Ionic liquid. *Macromol. Rapid Commun.* **2017**, 38 (21), 1700415.
- (7) Pan, X.; Liu, T.; Kautz, D. J.; Mu, L.; Tian, C.; Long, T. E.; Yang, P.; Lin, F. High-performance N-methyl-N-propylpiperidinium bis-(trifluoromethanesulfonyl)imide/poly(vinylidene fluoride-hexafluoropropylene) gel polymer electrolytes for lithium metal batteries. *J. Power Sources* **2018**, 403, 127–136.
- (8) Nagasawa, J. i.; Matsumoto, H.; Yoshida, M. Highly Efficient and Specific Gelation of Ionic Liquids by Polymeric Electrolytes to Form Ionogels with Substantially High Gel-Sol Transition Temperatures

- and Rheological Properties Like Self-Standing Ability and Rapid Recovery. ACS Macro Lett. 2012, 1 (9), 1108–1112.
- (9) Isik, M.; Gracia, R.; Kollnus, L. C.; Tomé, L. C.; Marrucho, I. M.; Mecerreyes, D. Cholinium-Based Poly(ionic liquid)s: Synthesis, Characterization, and Application as Biocompatible Ion Gels and Cellulose Coatings. ACS Macro Lett. 2013, 2 (11), 975–979.
- (10) Jansen, J. C.; Friess, K.; Clarizia, G.; Schauer, J.; Izák, P. High Ionic Liquid Content Polymeric Gel Membranes: Preparation and Performance. *Macromolecules* **2011**, *44* (1), 39–45.
- (11) Shalu, S.; Singh, V. K.; Singh, R. K. Development of ion conducting polymer gel electrolyte membranes based on polymer PVdF-HFP, BMIMTFSI ionic liquid and the Li-salt with improved electrical, thermal and structural properties. *J. Mater. Chem. C* **2015**, 3 (28), 7305–7318.
- (12) Zehbe, K.; Kollosche, M.; Lardong, S.; Kelling, A.; Schilde, U.; Taubert, A. Ionogels Based on Poly(methyl methacrylate) and Metal-Containing Ionic Liquids: Correlation between Structure and Mechanical and Electrical Properties. *Int. J. Mol. Sci.* **2016**, *17* (3), 391.
- (13) Kim, Y. M.; Seo, D. G.; Oh, H.; Moon, H. C. A facile random copolymer strategy to achieve highly conductive polymer gel electrolytes for electrochemical applications. *J. Mater. Chem. C* **2019**, 7 (1), 161–169.
- (14) He, Y. Y.; Boswell, P. G.; Buhlmann, P.; Lodge, T. P. Ion gels by self-assembly of a triblock copolymer in an ionic liquid. *J. Phys. Chem. B* **2007**, *111* (18), 4645–4652.
- (15) Miranda, D. F.; Versek, C.; Tuominen, M. T.; Russell, T. P.; Watkins, J. J. Cross-Linked Block Copolymer/Ionic Liquid Self-Assembled Blends for Polymer Gel Electrolytes with High Ionic Conductivity and Mechanical Strength. *Macromolecules* **2013**, *46* (23), 9313–9323.
- (16) Mackanic, D. G.; Yan, X.; Zhang, Q.; Matsuhisa, N.; Yu, Z.; Jiang, Y.; Manika, T.; Lopez, J.; Yan, H.; Liu, K.; Chen, X.; Cui, Y.; Bao, Z. Decoupling of mechanical properties and ionic conductivity in supramolecular lithium ion conductors. *Nat. Commun.* **2019**, *10* (1), 5384.
- (17) Chereddy, S.; Aguirre, J.; Dikin, D.; Wunder, S. L.; Chinnam, P. R. Gel Electrolyte Comprising Solvate Ionic Liquid and Methyl Cellulose. *ACS Appl. Energy Mater.* **2020**, 3 (1), 279–289.
- (18) Ito, A.; Yasuda, T.; Yoshioka, T.; Yoshida, A.; Li, X.; Hashimoto, K.; Nagai, K.; Shibayama, M.; Watanabe, M. Sulfonated Polyimide/Ionic Liquid Composite Membranes for CO<sub>2</sub> Separation: Transport Properties in Relation to Their Nanostructures. *Macromolecules* **2018**, *51* (18), 7112–7120.
- (19) Hayashi, E.; Thomas, M. L.; Hashimoto, K.; Tsuzuki, S.; Ito, A.; Watanabe, M. Application of Protic Ionic Liquids to CO<sub>2</sub> Separation in a Sulfonated Polyimide-Derived Ion Gel Membrane. *ACS Appl. Polym. Mater.* **2019**, *1* (6), 1579–1589.
- (20) Lee, S.-Y.; Ogawa, A.; Kanno, M.; Nakamoto, H.; Yasuda, T.; Watanabe, M. Nonhumidified Intermediate Temperature Fuel Cells Using Protic Ionic Liquids. *J. Am. Chem. Soc.* **2010**, *132* (28), 9764–9773
- (21) Wang, Y.; Chen, Y.; Gao, J. W.; Yoon, H. G.; Jin, L. Y.; Forsyth, M.; Dingemans, T. J.; Madsen, L. A. Highly Conductive and Thermally Stable Ion Gels with Tunable Anisotropy and Modulus. *Adv. Mater.* **2016**, 28 (13), 2571–2578.
- (22) Fox, R. J.; Yu, D.; Hegde, M.; Kumbhar, A. S.; Madsen, L. A.; Dingemans, T. J. Nanofibrillar Ionic Polymer Composites Enable High-Modulus Ion-Conducting Membranes. *ACS Appl. Mater. Interfaces* **2019**, *11* (43), 40551–40563.
- (23) Bostwick, J. E.; Zanelotti, C. J.; Iacob, C.; Korovich, A. G.; Madsen, L. A.; Colby, R. H. Ion Transport and Mechanical Properties of Non-Crystallizable Molecular Ionic Composite Electrolytes. *Macromolecules* **2020**, *53* (4), 1405–1414.
- (24) Wang, Y.; He, Y.; Yu, Z.; Gao, J.; ten Brinck, S.; Slebodnick, C.; Fahs, G. B.; Zanelotti, C. J.; Hegde, M.; Moore, R. B.; Ensing, B.; Dingemans, T. J.; Qiao, R.; Madsen, L. A. Double helical conformation and extreme rigidity in a rodlike polyelectrolyte. *Nat. Commun.* **2019**, *10* (1), 801.

- (25) Yu, Z.; He, Y.; Wang, Y.; Madsen, L. A.; Qiao, R. Molecular Structure and Dynamics of Ionic Liquids in a Rigid-Rod Polyanion-Based Ion Gel. *Langmuir* **2017**, *33* (1), 322–331.
- (26) Howlett, P. C.; MacFarlane, D. R.; Hollenkamp, A. F. High lithium metal cycling efficiency in a room-temperature ionic liquid. *Electrochem. Solid-State Lett.* **2004**, *7* (5), A97–A101.
- (27) Rodrigues, M.-T. F.; Kalaga, K.; Gullapalli, H.; Babu, G.; Reddy, A. L. M.; Ajayan, P. M. Hexagonal Boron Nitride-Based Electrolyte Composite for Li-Ion Battery Operation from Room Temperature to 150 °C. Adv. Energy Mater. 2016, 6 (12), 1600218.
- (28) Cho, J. H.; Lee, J.; Xia, Y.; Kim, B.; He, Y. Y.; Renn, M. J.; Lodge, T. P.; Frisbie, C. D. Printable ion-gel gate dielectrics for low-voltage polymer thin-film transistors on plastic. *Nat. Mater.* **2008**, 7 (11), 900–906.
- (29) Uk Hong, S.; Park, D.; Ko, Y.; Baek, I. Polymer-ionic liquid gels for enhanced gas transport. *Chem. Commun.* **2009**, No. 46, 7227–7229.
- (30) Tang, B.; Schneiderman, D. K.; Zare Bidoky, F.; Frisbie, C. D.; Lodge, T. P. Printable, Degradable, and Biocompatible Ion Gels from a Renewable ABA Triblock Polyester and a Low Toxicity Ionic Liquid. ACS Macro Lett. 2017, 6 (10), 1083–1088.
- (31) Rubinstein, M.; Colby, R. H. *Polymer Physics*; Oxford University Press: Oxford, 2003.
- (32) Gao, J.; Wang, Y.; Norder, B.; Garcia, S. J.; Picken, S. J.; Madsen, L. A.; Dingemans, T. J. Water and sodium transport and liquid crystalline alignment in a sulfonated aramid membrane. *J. Membr. Sci.* **2015**, 489, 194–203.
- (33) Sarkar, N.; Kershner, L. D. Rigid rod water-soluble polymers. *J. Appl. Polym. Sci.* **1996**, 62 (2), 393–408.
- (34) Wang, Y.; Gao, J. W.; Dingemans, T. J.; Madsen, L. A. Molecular Alignment and Ion Transport in Rigid Rod Polyelectrolyte Solutions. *Macromolecules* **2014**, *47* (9), 2984–2992.
- (35) Fishel, K.; Qian, G.; Benicewicz, B. C. PBI membranes via the PPA process. In *High Temperature Polymer Electrolyte Membrane Fuel Cells*; Springer: 2016; pp 217–238.
- (36) Padmanabhan, V.; Kumar, S. K. Gelation in semiflexible polymers. *J. Chem. Phys.* **2011**, *134* (17), 174902.
- (37) Zhou, Q.; Boyle, P. D.; Malpezzi, L.; Mele, A.; Shin, J.-H.; Passerini, S.; Henderson, W. A. Phase Behavior of Ionic Liquid—LiX Mixtures: Pyrrolidinium Cations and TFSI— Anions Linking Structure to Transport Properties. *Chem. Mater.* **2011**, 23 (19), 4331—4337.
- (38) Henderson, W. A.; Passerini, S. Phase Behavior of Ionic Liquid-LiX Mixtures: Pyrrolidinium Cations and TFSI- Anions. *Chem. Mater.* **2004**, *16* (15), 2881–2885.
- (39) Kunze, M.; Jeong, S.; Paillard, E.; Winter, M.; Passerini, S. Melting Behavior of Pyrrolidinium-Based Ionic Liquids and Their Binary Mixtures. *J. Phys. Chem. C* **2010**, *114* (28), 12364–12369.
- (40) MacFarlane, D. R.; Meakin, P.; Sun, J.; Amini, N.; Forsyth, M. Pyrrolidinium Imides: A New Family of Molten Salts and Conductive Plastic Crystal Phases. *J. Phys. Chem. B* **1999**, *103* (20), 4164–4170.
- (41) Song, J. Y.; Wang, Y. Y.; Wan, C. C. Review of gel-type polymer electrolytes for lithium-ion batteries. *J. Power Sources* **1999**, 77 (2), 183–197.
- (42) Long, L.; Wang, S.; Xiao, M.; Meng, Y. Polymer electrolytes for lithium polymer batteries. *J. Mater. Chem. A* **2016**, *4* (26), 10038–10069.
- (43) Liang, S.; Yan, W.; Wu, X.; Zhang, Y.; Zhu, Y.; Wang, H.; Wu, Y. Gel polymer electrolytes for lithium ion batteries: Fabrication, characterization and performance. *Solid State Ionics* **2018**, *318*, 2–18. (44) Yu, D.; Pan, X.; Bostwick, J. E.; Zanelotti, C. J.; Mu, L.; Colby, R. H.; Lin, F.; Madsen, L. A. Room Temperature to 150 °C Lithium Metal Batteries Enabled by a Rigid Molecular Ionic Composite

Electrolyte. Adv. Energy Mater. 2021, 11 (12), 2003559.